Check for updates

A novel modular modeling approach for understanding different electromechanics between left and right heart in rat

Nari Kim[1,2]*, Julius D. Pronto[1,2], David P. Nickerson[3], Andrew J. Taberner[3] and Peter J. Hunter[3]

[1]NLRL for Innovative Cardiovascular Engineering, Department of Physiology, College of Medicine, Inje University, Busan, South Korea, [2]Cardiovascular and Metabolic Disease Center, Inje University, Busan, South Korea, [3]Auckland Bioengineering Institute, The University of Auckland, Auckland, New Zealand

While ion channels and transporters involved in excitation-contraction coupling have been linked and constructed as comprehensive computational models, validation of whether each individual component of a model can be reused has not been previously attempted. Here we address this issue while using a novel modular modeling approach to investigate the underlying mechanism for the differences between left ventricle (LV) and right ventricle (RV). Our model was developed from modules constructed using the module assembly principles of the CellML model markup language. The components of three existing separate models of cardiac function were disassembled as to create smaller modules, validated individually, and then the component parts were combined into a new integrative model of a rat ventricular myocyte. The model was implemented in OpenCOR using the CellML standard in order to ensure reproducibility. Simulated action potential (AP), Ca^{2+} transient, and tension were in close agreement with our experimental measurements: LV AP showed a prolonged duration and a more prominent plateau compared with RV AP; Ca^{2+} transient showed prolonged duration and slow decay in LV compared to RV; the peak value and relaxation of tension were larger and slower, respectively, in LV compared to RV. Our novel approach of module-based mathematical modeling has established that the ionic mechanisms underlying the APs and Ca^{2+} handling play a role in the variation in force production between ventricles. This simulation process also provides a useful way to reuse and elaborate upon existing models in order to develop a new model.

KEYWORDS

modular modeling, electromechanics, interventricular difference, stress, Ca^{2+} modulation

Introduction

Mathematical modeling is a powerful technique that can improve one's understanding of normal and pathophysiology by incorporating a wealth of biological data that many researchers have accumulated. Using this comprehensive set of experimental data, many biophysical cell models have been developed to investigate the effect of subcellular changes on overall organ function, and many frameworks for simulation have been proposed. Most researchers want to share existing models and extend them into large-scale models that address the complexity at the whole cell level. As complex models need to be developed efficiently, many kinds of simulation tools have been developed. Among them, CellML, a model encoding format, has a couple of strengths. *1)* It uses MathML to represent the mathematics of the model in a way that both humans and computers can read (Terkildsen et al., 2008). *2)* The component instance and encapsulation layers (Cooling et al., 2016) allow modular configuration of the model to provide model scalability and model reuse.

The treatment of cardiovascular disease is shifting the paradigm from correcting a patient's deranged hemodynamic factors to blocking the most potent active signaling pathways in the disease. Accordingly, the strategy of cardiovascular disease research has turned to exploring ways to improve outcomes by modulating active signaling pathways through identification of relevant biochemical mechanisms, and most drug targets are membrane-bound proteins for cell signaling. Cellular signaling, on the other hand, integrates the behavior of many biological components, so it is not possible to gain mechanistic insights solely from knowledge of individual system components. Validated computational models can be dissected in time, physical space or parametric space, allowing the cellular and subcellular processes underlying normal or abnormal tissue and organ function to be validated at levels that cannot be achieved experimentally (Clayton, 2001). Therefore, there is a need for a computer model to investigate the physiological and pathophysiological mechanisms of normal and abnormal cardiovascular function in parallel with experimental studies.

The differences in the contractile performance between the left ventricle (LV) and the right ventricle (RV) based on their geometries have been examined in normal heart as well as diseased heart. In addition, distinct differences in the adaptive response of each ventricular cell have been observed in pathological conditions. However, clinical approaches to improving cardiac performance can be equally applicable to the LV and the RV in various forms of heart disease and are based on a general understanding of the laws that define cardiac mechanics. In practice, appropriate therapies for LV dysfunction have been shown to be not necessarily ideal for RV dysfunction (Walker and Buttrick, 2009). Therefore, a comprehensive understanding of the differences in the contractile performance between the LV and the RV myocytes in the normal heart as well as the diseased heart is important for improvement of existing therapeutics for various cardiovascular diseases.

Myocardial wall stress is the integration of the tension of individual myocardial fibers and is determined by the left ventricular cavity and wall dimensions (Laplace law) as well as ventricular pressure (Chowienczyk and Shah, 2012). These ventricular pressures and volumes show the length dependence of the contractile force (Frank-Starling effect) and are interdependent as a result of the inverse relationship between force generation and shortening velocity in the muscle. Thus, different myocardial wall stresses (or wall tensions) may result in different contractile properties in the LV and RV of a normal heart. During cardiac contraction, the wall stress increases as the myofilaments undergo cross-bridge cycling. The sequence of this excitatory-contraction coupling is similar between LV and RV, but the relative contributions of ion channels vary, affecting their action potential and ultimately their contractile behavior (Kim et al., 2010). In addition, ventricular wall stress determines oxygen consumption, cardiac hypertrophy response, and hepatic fibrosis. Quantification of ventricular wall stress is necessary to understand normal and pathological ventricular mechanics (Yin, 1981). Clinically, normalization of wall stress in volume/pressure-loaded heart disease has been considered a feedback mechanism that governs the rate and extent of development of ventricular hypertrophy (Hood et al., 1968; Grossman et al., 1975; Alter et al., 2012). Therefore, understanding the ventricular wall stress can provide important insights into the underlying ventricular mechanics and energetics in compromised hearts.

In this study, we performed quasi-isometric contraction experiments to compare different stresses in LV and RV muscles and Ca^{2+} imaging experiments for comparing different Ca^{2+} modulation between LV and RV myocytes. Then we implemented a mathematical model, first building a component model of individual transmembrane currents involved in the excitation-contraction (EC) coupling process, testing whether they function as an independent working model, and then combining them into a new integrative model of rat ventricular myocytes. The integrative model as well as modular model constituents were validated based on the experimental data and aided in drawing conclusions.

Materials and methods

Animal and ethics statement

Male Wistar rats (280–380 g) were used in this study. All experimental procedures were performed according to the requirements of the Animal Ethics Committee of the University of Auckland (Approval R595 and R787) and the National Animal Ethics Advisory Committee (The Animal

Welfare Act 1999; Schedules 1 to 7) as well as the protocol approved by the Institutional Review Board of Animals of Inje University College of Medicine.

Experimental procedures

Each experimental procedure was carried out with the same ways of previous studies. Briefly, the rats were anesthetized with isoflurane mixed in 100% O_2. The heart was quickly excised after cervical dislocation, placed in cold saline solution, and then perfused with an oxygenated solution of either low-calcium Tyrode's solution containing 2,3-butanedione monoxime (BDM) or normal Tyrode's solution, for trabecular muscles preparation or single cardiomyocytes preparation, respectively. In mechanical experiments, we measured active stress production of trabecular muscles from the LV and RV free wall using our mechanical testing device (Han et al., 2009). In Ca^{2+} transient experiments, we measured Ca^{2+} ion flux of single cardiomyocytes from the left and right midventricular wall using the ion-specific probe Fluo-4 AM (Invitrogen, Eugene, OR, United States) (Kim et al., 2012). In electrophysiological experiments, we measured action potentials of single cardiomyocytes from the left and right midventricular wall using the patch-clamping technique (Kim et al., 2010).

Model development

EC coupling is the process that links an action potential (electric excitation of cell membrane) to contraction (shortening and force development) of the heart. Action potential (AP) is caused by different ions crossing the plasma membrane through various ion channels and transporters. This electric excitation of the sarcolemma/ T-tubule induce Ca^{2+} release from sarcoplasmic reticulum (SR) via Ca^{2+}-induced Ca^{2+} release (CICR). Then free Ca^{2+} binds to the troponin complex, which facilitates the interaction of actin and myosin and contraction takes place. A schematic diagram of major ion currents and Ca^{2+} handling proteins, myofibrillar proteins are shown in Supplementary Figure S1. All the ionic processes and compartments in the whole cell model were used as modules and addressed briefly as described below. Our model retains the fundamental features of cardiomyocyte electrophysiology originally described by Pandit et al. (Pandit et al., 2001), detailed Ca^{2+} dynamics originally described by Hinch et al. (Hinch et al., 2004), and active contraction originally described by Niederer et al. (Niederer et al., 2006) in the rat heart: 1) the model formulations of the Na^+ channel, the Ca^{2+}-independent K^+ channel, the steady-state K^+ channel, the inward rectifier K^+ channel, the hyperpolarizing-activated channel, the background K^+ channel, the background Na^+ channel, the Na^+-K^+ pump, and the calmodulin were extracted from the Pandit et al. model; 2) the model formulations of the Ca^{2+} release unit, the Ca^{2+} pump, the Na^+-

Ca^{2+} exchanger, and the background Ca^{2+} channel were extracted from the Hinch et al. model; 3) the model formulation of the troponin, the tropomyosin, and the cross-bridge kinetics were extracted from the Niederer et al. model; 4) the model parameters and variables were adjusted to match the experimental observations, as described in the section below. The model also accounts for dynamic changes in ionic concentrations and fluxes during the action potential.

Based on our design principles for modularity in CellML (Cooling et al., 2016), we disassembled the components of the three separate models listed above and to produce individual working and testable modules. These modules which encompass variables and mathematics were implemented as CellML components and were independently tested and validated. Individual components are available online (https://models. physiomeproject.org/workspace/25c): INa_Pandit, Ito_Pandit, Iss_Pandit, IK1_Pandit, If_Pandit, IBNa_Pandit, IBK_Pandit, INaK_Pandit, CaRU_Hinch, ICaPump_Hinch, INCX_Hinch, IBCa_Hinch, ISRCaLeak_Hinch, ISERCA_Hinch, Icalmodulin_New, Itroponin_NSH, Itropomyosin _NSH, CrossBridge_NSH. In turn we combined the validated modules into a new integrative model of a rat ventricular myocyte using standard unit and universal constant modules. This model was validated against the experimental data. CellML text code for units are illustrated in Supplement 1. All model equations and parameter values are provided in Supplement 2. All simulations were performed using the OpenCOR desktop application version 0.3 (Garny and Hunter, 2015).

Formulation and validation of the individual model modules

The electrophysiological behavior can be described by the ordinary differential equation:

$$\frac{dV}{dt} = -\frac{I_{ion} + I_{stim}}{C_m}$$

where V is voltage, t is time, I_{ion} is the sum of all transmembrane ionic currents, I_{stim} is the externally applied stimulus current, and C_m is cell capacitance per unit surface area.

Na^+ current (I_{Na}) module

I_{Na} is responsible for upstroke of the AP. The formulation of I_{Na} model is from Pandit et al. (2001) and the CellML text code for I_{Na} model is as shown in Supplement 1. I_{Na} kinetics were reported to be similar across different species, giving us a rationale to use these variables: the steady-state activation and inactivation curves, the normalized peak current-voltage (I-V) relationship, and the maximum Na^+ conductance (g_{Na}) are based and adjusted from the rat study (Lee et al., 1999); the time constants for activation (τ_m) and inactivation (τ_h, τ_j) used as model parameters were adapted from the guinea pig study (Luo
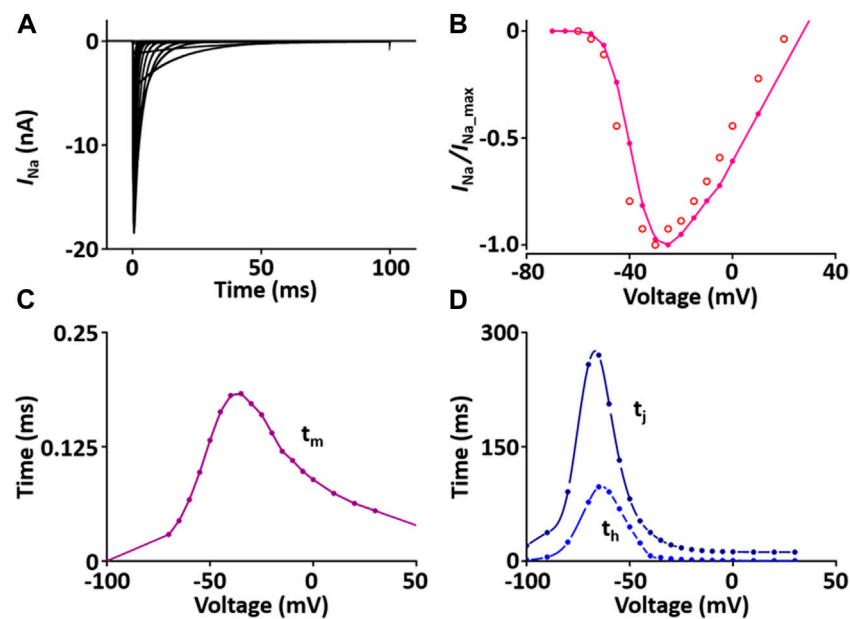
FIGURE 1
Verification of I_{Na} implementation (Kim, 2018). **(A)** Simulated current traces of the Na$^+$ channel. **(B)** Normalized simulated *I-V* relationship of I_{Na} (o represents experimental data from Lee et al., 1999). **(C)** Simulated activation time constant (τ_m). **(D)** Simulated inactivation time constants (τ_h, τ_j).

and Rudy, 1994) and scaled. The m-gate, h-gate, and j-gate of three gates for I_{Na} were encapsulated and embedded inside the sodium channel. We used OpenCOR, with end point 40 ms and Point interval 0.1 ms, to solve the equations for I_{Na} under several voltage steps in one fixed condition with [Na$^+$]$_o$ = 145 mM and [Na$^+$]$_i$ = 11.28 mM. We obtained numerical values for all variables and saved them as comma-separated values (CSV) files and then plotted whole-cell current traces, the *I-V* relationship and time constants, which corresponded well with published results (Figure 1).

Each module was modeled in the same way and the values were compared with the experimental data or the results of the other studies.

Ca^{2+}-independent transient outward K$^+$ current (I_{to}) module

I_{to} contributes to the notch configuration of the AP. The formulation of the I_{to} model is from Pandit et al. (2001) and is shown in Supplement 2. All values of the I_{to} model are based on individual experimental data from the rat heart: the steady-state activation and inactivation values are from Stengl et al. (Stengl et al., 1998); the time constant for activation from Angus et al. (Agus et al., 1991); the inactivation time constants from Wettwer et al. (Wettwer et al., 1993); and the recovery time constants from Volk et al. (Volk et al., 1999). In one fixed condition with [K$^+$]$_o$ = 5.4 mM and [K$^+$]$_i$ = 138.72 mM, the current traces and parameters of I_{to} corresponded well to published results (Figure 2).

Steady-state outward K$^+$ current (I_{ss}) module

I_{ss} contributes to the repolarization of the AP. The formulation of the I_{ss} model is from Pandit et al. (2001) and is as shown in Supplement 2. All values of the I_{ss} model are based on individual experimental data in the rat heart: the steady-state activation and inactivation values from Weis et al. (Weis et al., 1993); the time constant for activation, which is 10 times slower than that of I_{to}, from Apkon and Nerbonne (Apkon and Nerbonne, 1991); the time constant for inactivation from Berger et al. (Berger et al., 1998). In one fixed condition with [K$^+$]$_o$ = 5 mM and [K$^+$]$_i$ = 140.45 mM, the current traces and parameters of I_{ss} corresponded well with published results (Figure 3). Values for I_{ss} were obtained at the end of a long (300 ms) depolarized voltage clamp pulse.

Inward rectifier K$^+$ current (I_{K1}) module

I_{K1} stabilizes the resting membrane potential. The formulation of I_{K1} model is from Pandit et al. (2001) and is as shown in Supplement 2. To characterize I_{K1} depending on [K$^+$]$_o$, current traces and *I-V* relationship of I_{K1} were verified in condition with [K$^+$]$_o$ = 5.4 mM or 10 mM, which corresponded well with published results (Figures 4A,B).

Hyperpolarization-activated current (I_f) module

I_f is activated when the membrane is hyperpolarized from the resting potential and modulates the AP. The formulation of I_f model is from Demir et al. (Demir et al., 1994) and the values are
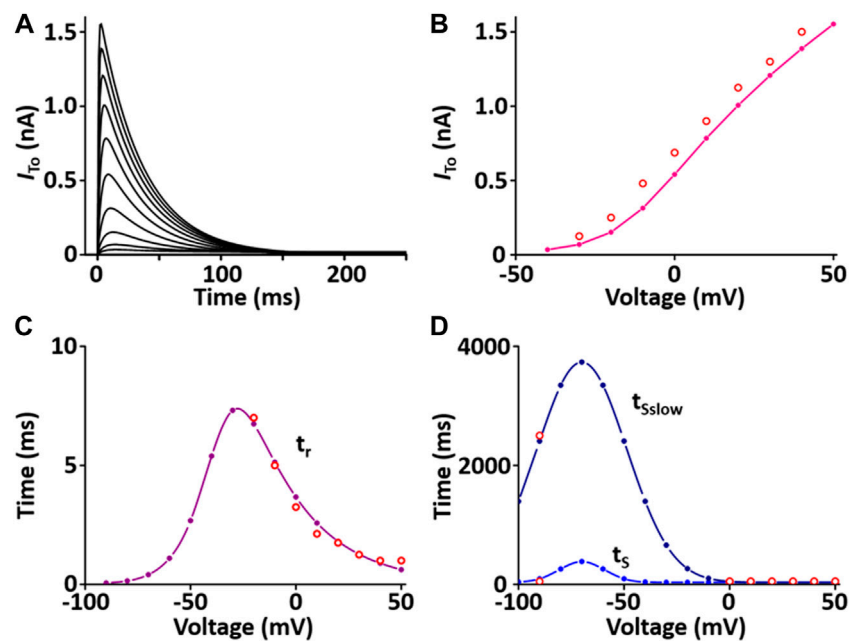
FIGURE 2
Verification of I_{to} implementation (Kim, 2018). **(A)** Simulated current traces of Ca^{2+}–independent transient outward K^+ channel. **(B)** Simulated I-V relationship for I_{to} (pink line). This simulated result is in close agreement with representative experimental result (o, Clark et al., 1995). **(C)** Simulated activation time constant (τ_r, purple line). This simulated result is in close agreement with the representative experimental result (o, Agus et al., 1991). **(D)** Simulated inactivation time constants (τ_S, τ_{Sslow}, blue lines). This simulated result is in close agreement with the representative experimental result (o, Wettwer et al., 1993).

based on experimental data from previous studies (Demir et al., 1994; Cerbai et al., 1996; Fares et al., 1998) and is as shown in Supplement 2. To verify the I_f model, the extracellular condition is to set $[K^+]_o$ and $[Na^+]_o$ at 25 and 30 mM, respectively, and the intracellular condition sets $[K^+]_i$ and $[Na^+]_i$ at 130 and 2 mM, respectively. Current traces and I-V relationship of I_f were corresponded closely with published results (Figures 4C,D).

Background Na^+ current (I_{BNa}) module

The formulation of I_{BNa} model is from the Pandit et al. (2001) model and is as shown in Supplement 2. The magnitude is adjusted based on experimental data from Demir et al. (1994).

Background K^+ current (I_{BK}) module

The formulation of I_{BK} model is from the Pandit et al. (2001) model and is as shown in Supplement 2. The magnitude is adjusted based on experimental data from Demir et al. (1994).

Na^+/K^+ pump current (I_{NaK}) module

I_{NaK} directly produces a small potential difference, which causes the membrane potential to be negative. The formulation of I_{NaK} model is that of the Pandit et al. (2001) model adapted from earlier work by Luo and Rudy (1994) and is as shown in Supplement 2. When normalized to 100 pF, the I_{NaK} model was 0.195 A·F^{-1} at 0 mV, which is close to the value of 0.2 A·F^{-1} at

0 mV in the experimental data of Stimers and Dobretsov (Stimers and Dobretsov, 1998) (Figure 5).

Ca^{2+} release unit (CaRU) module

The CaRU consists of one L-type Ca^{2+} channel (LCC) and ryanodine receptors (RYRs) and transports Ca^{2+} ions in the dyadic subspace between the T-tubules and the sarcoplasmic reticulum (SR). LCCs are located in sarcolemmal membrane and T-tubules and carries Ca^{2+} ions in the inward direction when the membrane is depolarized. RYRs are located in SR and release Ca^{2+} from SR *via* physical coupling to LCCs. These two channels induce to increase the cytosol Ca^{2+}. The formulation of the LCC and RYRs models are from the Hinch et al. (2004) model, which is simplified by six coupled ordinary differential equations for Ca^{2+}-induced Ca^{2+} release: *1)* the 3-state model of the LCC is based on Jafri et al. (Jafri et al., 1998) study and the 3-state model for RYR is based on Stengl et al. (1998) study; *2)* the 3-state LCC and the 3-state RYR models were combined to form a 9-state model, which was simplified further to produce a 4-state model of the CaRU. All parameters and functions of the CaRU model are shown in Supplement 2. To verify the CaRU model, the current traces and peak I-V relationship of the Ca^{2+} channel were obtained by various voltage steps from a holding potential of −50 mV in one fixed condition with $[Ca^{2+}]_o$ = 1.2 mM, which was compared with that measured experimentally.
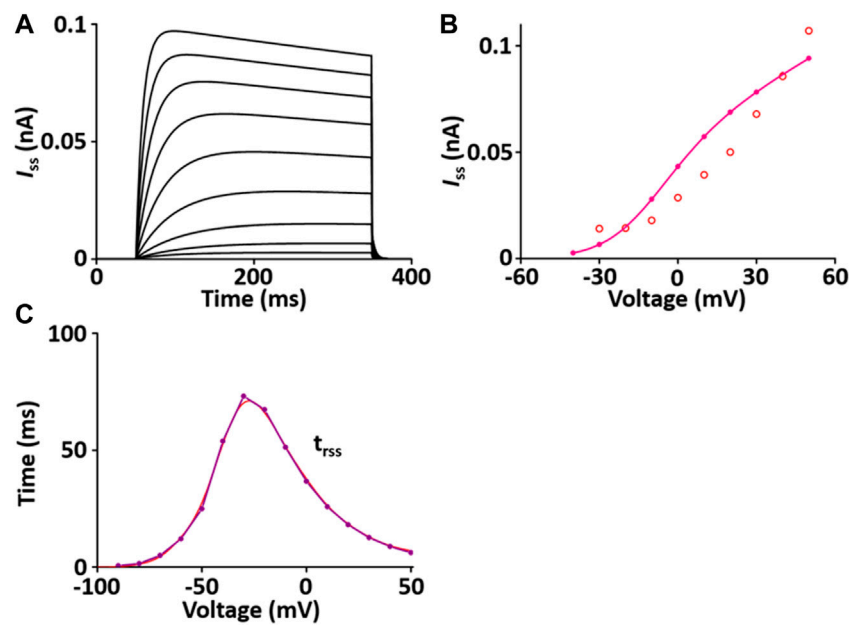
FIGURE 3
Verification of I_{ss} implementation (Kim, 2018). **(A)** Simulated current traces of the steady-state outward K$^+$ channel. **(B)** Simulated I-V relationship of I_{ss} (pink line). This simulated result is in close agreement with the representative experimental result (o, Clark et al. (1995)). **(C)** Simulated activation time constant (τ_{rss}, purple line). This simulated result is in close agreement with the representative experimental result (red line, Apkon and Nerbonne (1991)), which is 10 times slower than the corresponding one for I_{to} (Figure 3C).

Simulated and measured currents were normalized to make the peak value of both equal to 1 at 0 mV, and both I-V curves are in close agreement. One feature of Ca^{2+} release is that the peak of I_{RYR} is shifted by ~10 mV in the hyperpolarizing direction relative to that of I_{LCC}, which is well simulated. Furthermore, EC coupling gain decreases as membrane voltage increases. This feature of simulated result corresponded well to published results (Figure 6).

Ca^{2+} pump current module

Sarcolemmal Ca^{2+} pump actively transports Ca^{2+} outward and SR Ca^{2+} pump actively transports Ca^{2+} from the cytosol into the SR lumen. These two pumps induce to decrease the cytosol Ca^{2+}. The formulations of the SR Ca^{2+} pump, SERCA current (I_{SERCA}) model and the sarcolemmal Ca^{2+} pump current (I_{pCa}) model are from the Hinch et al. (2004) model and is as shown in Supplement 2. To verify the I_{SERCA} model, the Ca^{2+} dependence of SERCA activity was generated and compared with experimental data (Figure 7A)

Na$^+$-Ca^{2+} exchanger current (I_{NCX}) module

Na$^+$-Ca^{2+} exchanger (NCX) exchanges 1 internal Ca^{2+} ion for three external Na$^+$ ions *via* a membrane carrier. The formulation of the I_{NCX} model is from the Hinch et al. (2004) model and is as shown in Supplement 2. To verify I_{NCX}, the extracellular

condition set [Ca^{2+}]$_o$ and [Na$^+$]$_o$ at 1 and 140 mM, respectively, and the intracellular condition set [Na$^+$]$_i$ and free [Ca^{2+}]$_i$ at 20 and 1.2 mM, respectively, based on experimental conditions by Li et al. (Li et al., 2013). The simulated I_{NCX} model was generated, and the model output (Figure 7B) shows close agreement with the experimental results of Li et al. (2013).

Background Ca^{2+} current (I_{BCa}) module

The formulations of the background Ca^{2+} current (I_{BCa}) model is from the Hinch et al. (2004) model and is as shown in Supplement 2.

## Calmodulin and troponin module

Ca^{2+} is buffered by calmodulin and troponin in the cytosol. The calculation of buffering by calmodulin is from the Pandit et al. (2001) model and by troponin current (I_{TRPN}) model from the Niederer et al. (2006) model and is as shown in Supplement 2.

Tropomyosin module

Tropomyosin is situated in the actin groove and when it is shifted out of the actin groove, actin binds to myosin. The tropomyosin was characterized by the fraction of actin sites available for cross-bridge binding (z) and the formulation of z is from the Niederer et al. (2006) model and is as shown in Supplement 2.
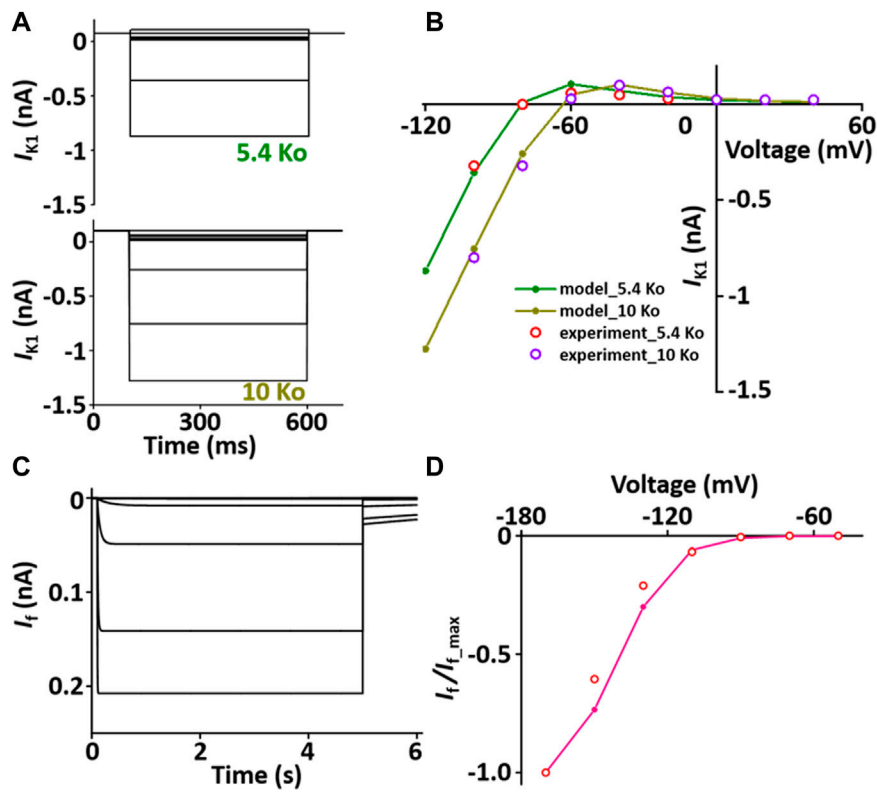
FIGURE 4
Verification of I_{K1} and I_f implementation (Kim, 2018). **(A)** Simulated current traces of the hyperpolarization-activated channel at extracellular K$^+$ ion concentrations of 5.4 mM (5.4 Ko) and 10 mM (10 Ko). **(B)** Normalized simulated I-V relationship for I_{K1} (olive and dark yellow lines). This simulated result is in close agreement with the representative experimental results (experiment_5.4 Ko, experiment_10 Ko) which were digitized from Pandit et al. (2001)). **(C)** Simulated current traces of the hyperpolarization-activated channel. **(D)** Normalized simulated I-V relationship for I_f (pink line). This simulated result is in close agreement with the representative experimental result (o, Fares et al. (Fares et al., 1998)).
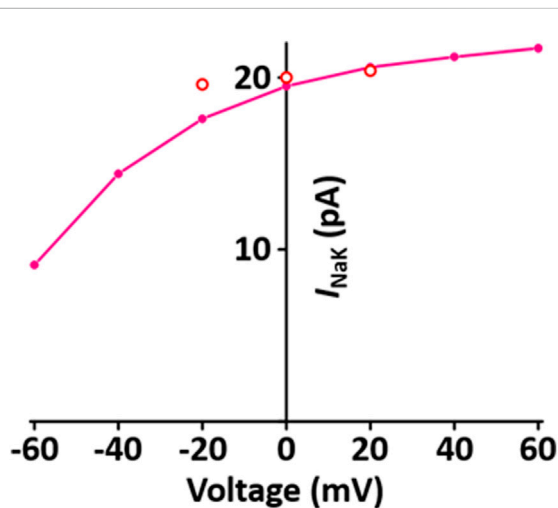
FIGURE 5
Verification of I_{NaK} implementation (Kim, 2018). Simulated I-V relationship for the sodium-potassium pump. o represents experimental data from Stimers and Dobretsov, 1998.

Cross-bridge module

As myosin head attaches and detaches from myosin-binding site on the actin, it makes the actin filaments closer together, thus shortening the length of the sarcomere. These length changes of the myofibrils produce tension (cardiac contraction). The formulations of the isometric tension (T) is from the Niederer et al., 2006 model assuming a "fading memory," and is as shown in Supplement 2. The fading memory model assumes that the current tension is influenced more by recent length changes than earlier length changes (Hunter et al., 1998) and phenomenologically explains the relationship between tension and cross-bridge kinetics. Here tension development can be separated into nonlinear static and linear time-dependent components and tension development associated with cross-bridge kinetics is proportional to z. The ratio of the isometric tension to the maximum tension at full activation for the same sarcomere length is equal to the ratio of z to the fraction of actin sites available at full activation for a given sarcomere length.
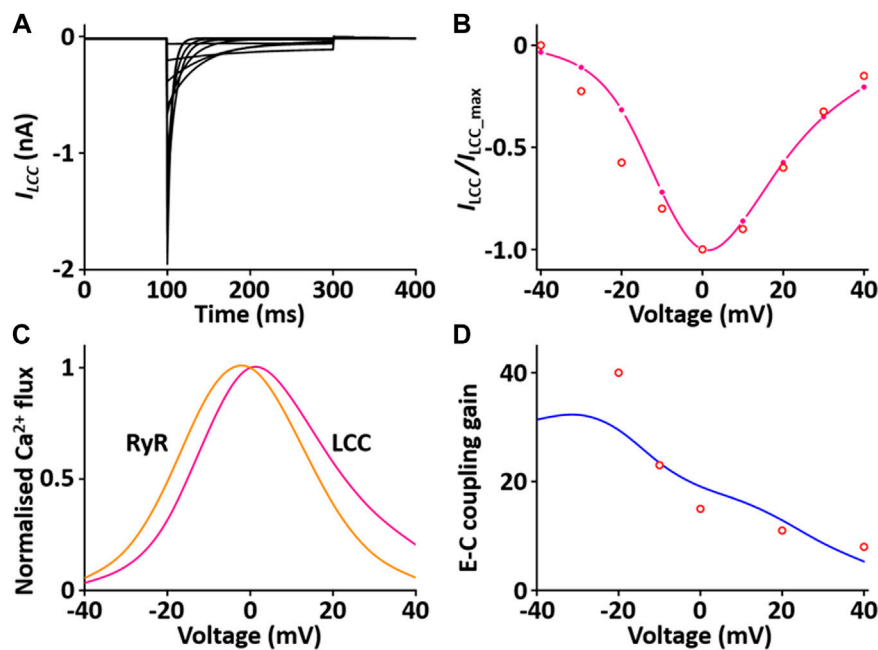
FIGURE 6
Verification of I_{LCC} and I_{RYR} implementation (Kim, 2018). **(A)** Simulated current traces for the LCC by a voltage step from −40 to 40 mV from a holding potential of −50 mV. **(B)** Normalized simulated *I-V* relationship for I_{LCC} (pink line). This simulated result is in close agreement with representative experimental result (o, Zahradnikova et al. (Zahradnikova et al., 2004)). **(C)** Simulated peak fluxes of LCC (pink line) and RYR (yellow line) as a function of membrane voltage. **(D)** Simulated EC coupling gain (blue line, maximum of RYR flux/maximum LCC flux) is in close agreement with representative experimental result (o, Wier at al. (Wier et al., 1994)).
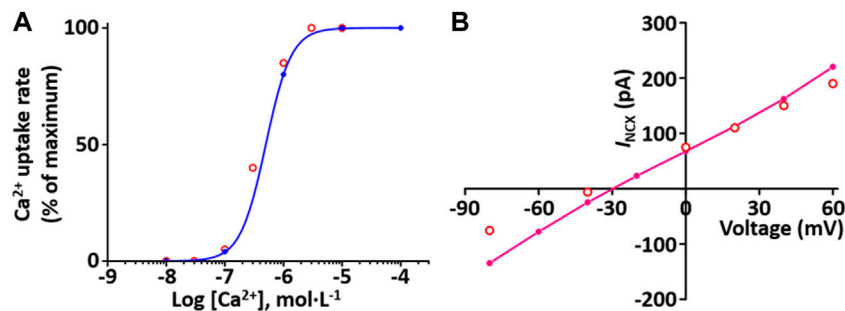

FIGURE 7
Verification of I_{SERCA} and I_{NCX} implementation (Kim, 2018). **(A)** The Ca^{2+} dependence of the relative rate of simulated SERCA activity is well plotted (blue line). This result is close agreement with representative experimental values (o, Lytton et al. (Lytton et al., 1992)). **(B)** Simulated *I-V* relationship for the NCX (pink line). This result is close agreement with representative experimental values (o, Li et al., 2013).

Incorporating all components to the biophysical whole cell model

We implemented all individual modules as CellML components and then, using the CellML model import facility in OpenCOR (http://www.opencor.ws/), we were able to compose the whole cell model, encompassing module variables and mathematics. Using the CellML model import facility allows to distribute these components among multiple files and to make in-memory copies of components from other files (Miller et al., 2010). The structure of the model, including separate files for units and component sets is shown in Figure 8.
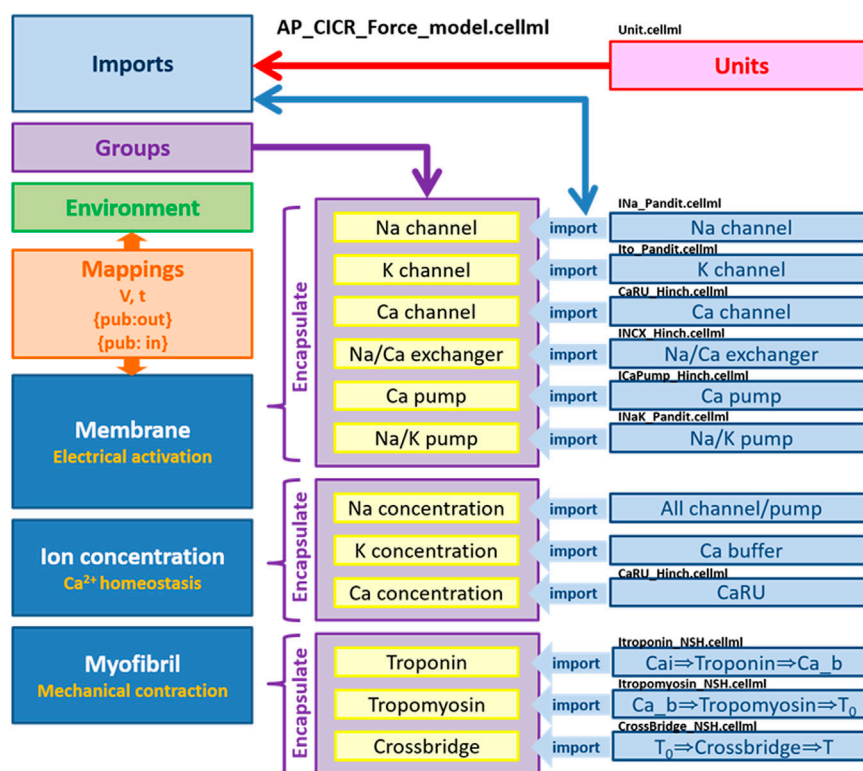
FIGURE 8
Overall structure of biophysical whole cell model (AP_CICR_Force_model) showing the encapsulation hierarchy (purple), the CellML model imports (blue) and the other key parts (units, components and mappings) of the top level CellML model (Kim, 2018).

When incorporating all components, we adjusted the I_{LCC} parameters based on previous results (Kim et al., 2010). The voltage at half-maximal activation was applied -15 mV and -10 mV for the LV and RV models, respectively. The formulation of I_{SERCA} obtained from the Hinch et al. (2004) model was adapted from earlier work by Jafri et al. (1998), so the maximum pump rate in their work is somewhat different from that in the rat. It is well known that the activity of SERCA is higher in the rat ventricle than in rabbit, ferret, dog, cat, guinea-pig and human ventricles (Bers, 2000). Therefore, g_{SERCA} was increased by 20% to achieve similar activity for rat SERCA. The parameters of the troponin and the tropomyosin modules were adjusted to values appropriate for 37°C: temperature has some effect on the affinity of Ca^{2+} for TnC (McCubbin et al., 1980) and the affinity of Ca^{2+} for TnC was increased by 0.13 when temperature was increased from 21 to 37°C (Gillis et al., 2000); the wide range of Q_{10} values have been reported in order to reveal temperature dependence of force development in various muscles (Peiper et al., 1975; Stein et al., 1982; Janssen et al., 2002), we used three of Q_{10} value to parameterization of relaxation rates of tropomyosin.

Results

Verification of biophysical whole cell simulation: Action potential and Ca²⁺ dynamics

The whole cell model which was implemented *via* the steps described above shows the phenotype of typical AP waveforms, I_{LCC}, and calcium transients in LV and RV myocytes (Supplementary Figure S2). Simulated AP waveforms are close agreement with our experimental recordings (Figure 9): the peak overshoot and duration of the simulated AP is very similar to the experimental recordings; the duration of simulated LV AP prolongs and the plateau phase of it is more prominent compared to the simulated RV AP. This result is in consistent with previous experimental results (Figure 9 and *see* Kaprielian et al., 2002; Kim et al., 2010; Stankovicova et al., 2000).

During the implementation of the cell model, one of the tuning parameters was the voltage at half-maximal activation of LCC, so it was necessary to compare the LCC characteristics between the LV and RV cells. The model-generated current-
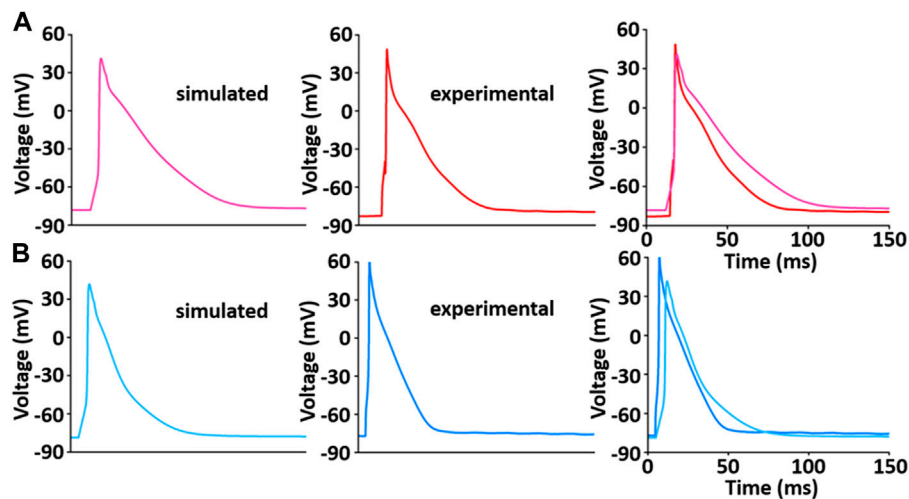
FIGURE 9
Model-generated LV **(A)** and RV **(B)** APs at 1 Hz and 22°C (Kim, 2018). Each simulated APs was validated with experimentally recorded LV **(A)** and RV **(B)** APs, respectively.
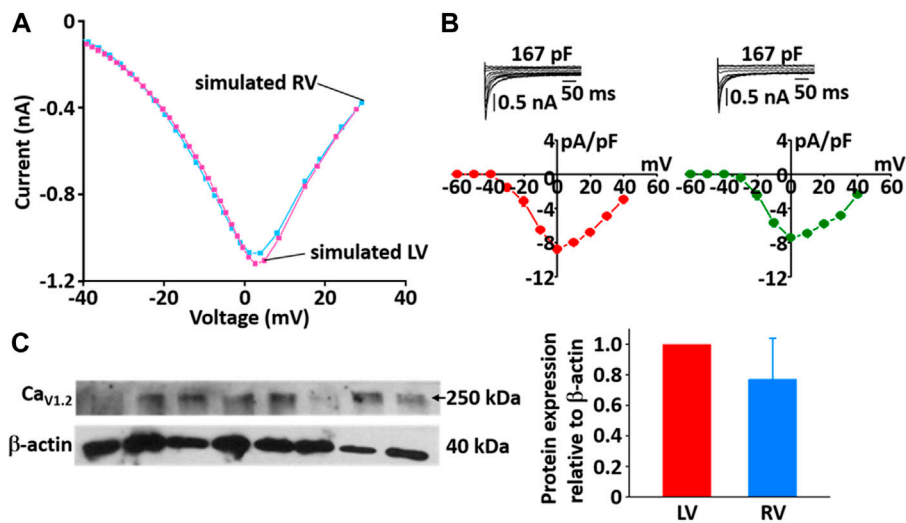
FIGURE 10
Comparison of *I-V* relationship of LCC in model **(A)** and experimental recordings **(B)** for LV and RV myocytes at 22°C (Kim, 2018). In panel **(B)**, inserts are representative ILCC traces from LV and RV myocytes and summary current-voltage relationships in LV ($n = 5$, red circles) and RV ($n = 4$, blue circles) myocytes, which from our previous study (Kim, Cannell et al., 2010). **(C)** Verification of protein expression of LCC proteins between LV and RV by immunoblotting. Representative blots and densitometric analysis of $Ca_{v1.2}$ (250 kDa, $n = 4$) with β-actin (42 kDa) as housekeeping protein.

voltage (*I-V*) curves of LCC in LV and RV myocytes conformed well to previous experimental observation (Figures 10A,B). Peak current in LV myocytes was slightly larger than that in RV myocytes and peak I_{LCC} occurred at ~0 mV in both LV and RV myocytes. However, as shown in Figure 10C, the protein expression of LCC is not different between the ventricles ($n = 4$; $p > 0.05$).

The simulated Ca^{2+} transients during the AP (Figure 11) conforms to the experimental observation that the Ca^{2+} decay is slower in LV than in RV myocytes (Figure 12), which could cause
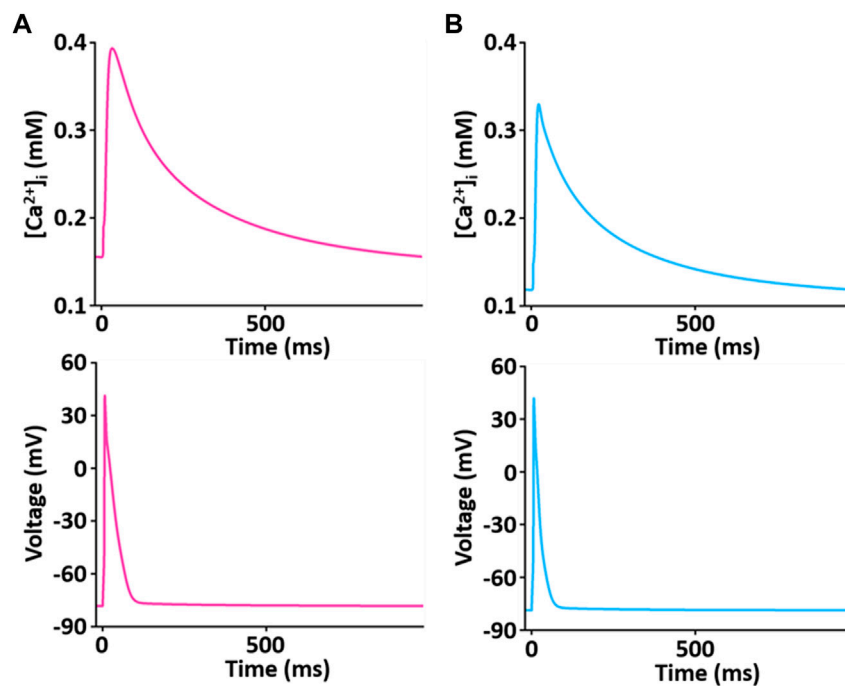
FIGURE 11
Simulated Ca^{2+} transient trace shows the underlying changes in [Ca^{2+}]$_i$ during corresponding AP duration for LV **(A)** and RV **(B)** myocytes at 1 Hz and 22°C (Kim, 2018).
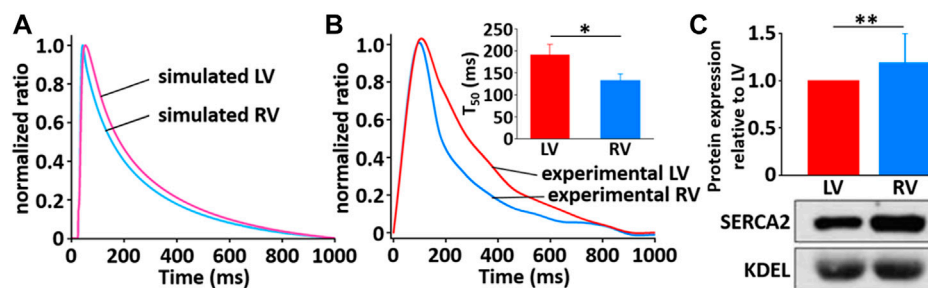

FIGURE 12
Comparison of normalized Ca^{2+} transients in model **(A)** and experimental recordings **(B)** for LV and RV myocytes at 1 Hz and 22°C (Kim, 2018). The peak ratio of the Ca^{2+} transients in the LV and RV myocytes was not different; however, the decay of the Ca^{2+} transients was much slower in LV than in RV myocyte: insert shows that T$_{50}$ of LV cells (190.1 ms $\pm$ 24.8 ms, $n = 6$) is significantly different from that of RV cells (132.8 ms $\pm$ 15.2 ms, $n = 6$). **(C)** Verification of protein expression of SERCA2a proteins between LV and RV by immunoblotting. Representative blots and densitometric analysis of SERCA2a (100 kDa, $n = 2$) with KDEL (78 kDa) as SR marker and housekeeping protein. The bar graphs indicate mean $\pm$ SEM. *$p < 0.05$, **$p < 0.001$.

a large Ca^{2+} flux in the LV myocyte. Moreover, we assumed that the activity of SERCA in RV myocytes is higher than in LV myocytes since time to 50% decay from peak (T$_{50}$) against [Ca^{2+}]$_i$ was significantly different between LV and RV myocytes ($\approx$30%) (Figure 12B insert and *see* Taylor et al., 2004). Furthermore, as shown in Figure 12C, we revealed that SERCA2a expression of the RV is higher than that of the LV ($n = 3$; $p < 0.001$). These results can explain the underlying mechanism of the different Ca^{2+} kinetics between the LV and RV well and provide a rationale for "fine tuning" the model parameters of SERCA activity obtained from the study of Hinch et al. (2004) to reproduce a biophysical whole cell model.
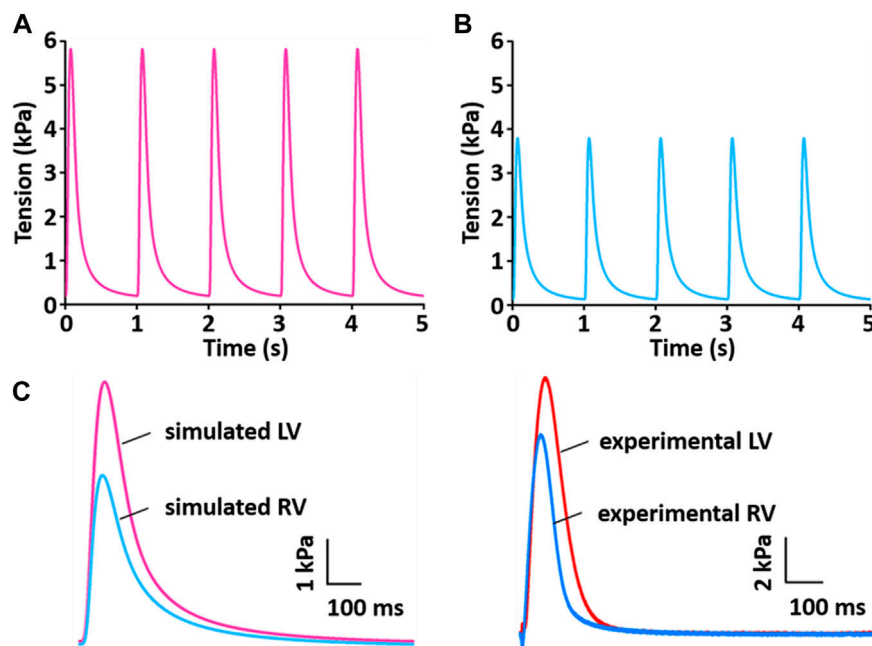
FIGURE 13
Model-generated tension production at 1 Hz and 37°C (Kim, 2018). **(A)** The tension traces for the LV model. **(B)** The tension traces for the RV model. **(C)** Comparison of simulated tension between LV and RV and validation of simulated tensions with experimentally recorded LV and RV tensions.
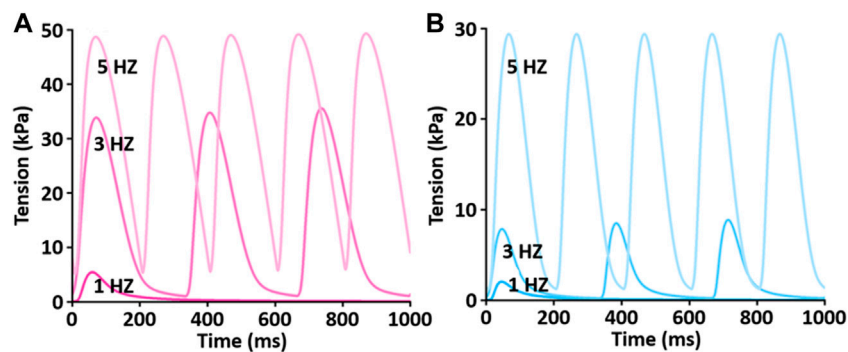
FIGURE 14
Comparison of SFR of simulated tension production between LV **(A)** and RV **(B)** myocytes at 1 Hz, 3 Hz, and 5 Hz and 37°C (Kim, 2018). Both active and passive tensions increase depending on stimulation frequency from 1 to 5 Hz.

Verification of biophysical whole cell simulation: Tension production

Figure 13 shows the simulation results for tension production over 5 s. The simulated tensions for LV and RV are in close agreement with the experimentally recorded results (Figure 13C): the peak and duration of the simulated tension are larger and

longer, respectively, in the LV than in the RV myocytes. However, there is a somewhat different magnitude of generated tension between simulated and experimental results.

To test the functionality of the model, the model was paced at 3 and 5 Hz. The results of simulated tensions showed the expected positive stress-frequency relationship (SFR) and their kinetics are close agreement with the experimentally recorded tensions (Figures 14, 15).

FIGURE 15
Comparison of traces for normalized tension between LV and RV myocytes at stimulations rates of 3 and 5 Hz (Kim, 2018). Black lines: experimental data. Colored lines: simulated results.
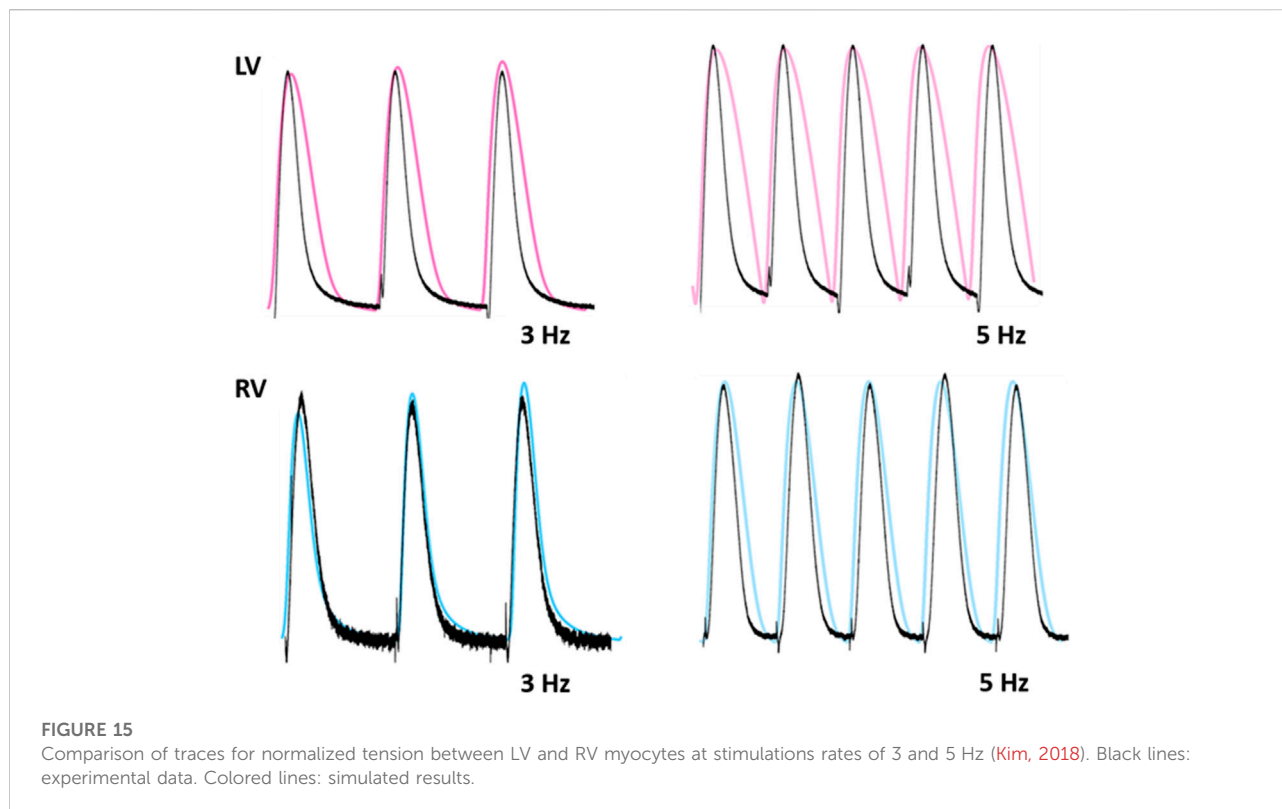
Discussion

This modeling approach serves as a good example of constructing complex models using the Physiome standard model protocol CellML in an efficient way to reuse constituents of existing computational models as modules. We assembled these reusable modules *via* component instances and encapsulation hierarchies to implement a comprehensive electromechanical model. Importantly, all modular models in this study could be subsumed into other models without modification, as each module component was constructed separately from the existing model and validated based on the results of previous related papers.

The present study is the first attempt to quantify and integrate a rat electromechanical model based on contractile proteins, as well as biophysical, experimentally derived components of ionic currents, transporters and Ca^{2+} modulators, to explain the underlying mechanisms for different stresses between LV and RV myocytes. Different AP waveforms produce different Ca^{2+} fluxes, which could be due to different SR Ca^{2+} loading and sequestration during AP. These simulation results explain why the LV exhibits greater stress compared to the RV, for which the prolonged AP duration and increased Ca^{2+} transients in the LV provide a plausible mechanism.

In this study, all simulated results of AP, LCC, Ca^{2+} transient, and tension were in close agreement with our those experimentally recorded. There is a somewhat different morphology of the APs between simulation and experiment. AP duration and shape vary from cell to cell, and may be because experimental and simulated conditions do not exactly match, or because rat AP configurations show a variation in duration and shape due to transmural heterogeneity of APs in most experiments (Stankovicova et al., 2000; Kim et al., 2010). However, it is shown that the shape of the simulated AP is very similar to experimentally recorded AP.

In adult rat ventricular myocytes, ~ 90% of the source of the Ca^{2+} transient is Ca^{2+} released from the SR (Bers, 2002), and subsequent Ca^{2+} sequestration by SERCA matches SR release. This gives us a rationale for using SERCA as the main contributor to explain the kinetics of Ca^{2+} transients. As shown in simulations describing the changes in $[Ca^{2+}]_i$ (*see also* Figures 11, 12), the kinetics of Ca^{2+} transient decay in the LV myocyte are much slower than those for the RV myocyte, whereas the peak ratio of the Ca^{2+} transient is not significantly different between ventricles. This result was very well reproduced by "fine tuning" the model parameters of SERCA activity obtained from the study of Hinch et al. (2004). In fact, the decline of the Ca^{2+} transient is regulated by SERCA as well as NCX. The parameterization of NCX activity may be considered, whereas >95% of this decline is due to

SERCA in rat myocytes (Milani-Nejad and Janssen, 2014). Therefore, the parameterization of SERCA activity is enough to prove the underlying mechanism for different Ca^{2+} transients between LV and RV myocytes. In addition, the underlying mechanism may be due in part to the fact that SERCA protein expression in the RV is higher than LV (Figure 12C). In the study of the force-frequency behavior of human myocardium, the protein level/activity of SERCA determines the systolic contractile reserves with respect to frequency potentiation of contractile force by playing a role in maintaining the SR load and regulating the cytosolic $[Ca^{2+}]$ during both systole and diastole (Hasenfuss et al., 1994).

Another specific aim for this simulation was to establish that the ionic mechanisms underlying the APs play a role in difference in force production between ventricles. The simulation results thus provide a good electromechanical link between the differences in Ca^{2+} handling and the corresponding tension changes. Under physiological conditions (37°C), force of contraction and speed of relaxation are complex. Thus using most variables based mainly on experimental data obtained at room temperature in the present model may limit its fidelity at 37°C, as temperature would significantly affect myofilament properties as well as Ca^{2+} handling (Janssen et al., 2002). However, even if the properties of troponin and tropomyosin and the activity of Ca^{2+} channel are adjusted, the model result is good enough to match the experimental results in this study (Figures 13–15). To verify distinct properties of contraction in the LV and RV, one of the possible ionic mechanisms, here VL of I_{LCC}, underlying the LV and RV APs was modified, providing a good electromechanical linkage between the differences in Ca^{2+} handling and the corresponding changes in peak tension and duration of contraction.

Furthermore, Ca^{2+} transporters involved in relaxation under physiological conditions (37°C) has been reported to be accelerated compared to that at room temperature due to differences in the temperature sensitivity of the involved systems (Puglisi et al., 1996; Mackiewicz and Lewartowski, 2006). Thus, the maximum pump rate of SERCA needs to be adjusted to 37°C using the Q_{10} adjustment factor (1.415) to generate tension production as well as SFR. Among Ca^{2+} transport systems, the modification of Ca^{2+} channels and SERCA is good enough to produce different contractility between the LV and RV, which could confirm their important contributors to contractility.

Limitations of the study and future work

In the present study, we suggested varying activity of SERCA as one of the underlying mechanisms that could contribute to the production of different stresses in the LV and RV. The activity of RYR should also be evaluated experimentally for a more comprehensive understanding of Ca^{2+} dynamics in the LV

and RV. In the same context, this model is somewhat limited to Ca^{2+}-dependent regulatory proteins such as CaMKII, calcineurin (CaN), phospholamban, and cAMP. These proteins alter the functions of multiple targets and thus are related to rate-dependent cellular response. LCC is influenced by Ca^{2+}-dependent inactivation and Ca^{2+}-dependent facilitation *via* activations of CaMKII and CaN (Pitt et al., 2001; Hudmon et al., 2005; Tandan et al., 2009). CaMKII and CaN also affect rate-dependent acceleration of relaxation *via* regulation of SERCA activity (Toyofuku et al., 1994; Munch et al., 2002). Therefore, future work is needed to implement individual modules of these proteins and then combine them with existing model.

During the diastolic phase, the myocardium stretches and passive tension is developed. Passive tension contributes to the diastolic wall tension, which determines the degree of ventricular filing and subsequent stroke volume (Allen and Kentish, 1985). At sarcomere lengths of 1.8–2.2 μm, titin and collagen are the most important contributors to passive tension (Granzier and Irving, 1995). Titin is a single giant polypeptide spanning from the Z disk to the M band region of sarcomere, with three isoforms. The isoform of titin varies with development and isoform variation causes the alteration of cardiac stiffness in the presence of heart diseases (Crocini and Gotthardt, 2021). In addition, cardiac stiffness is modulated by phosphorylation of titin by protein kinases. Therefore, in future study, it is necessary to develop a cross-bridge kinetic model that includes the role of titin.

In fact, cardiac muscle relaxation is a system-level characteristic, requiring fundamental integration of three governing systems: intracellular calcium decline, thin filament deactivation, and cross-bridge cycling kinetics (Danziger et al., 1990). Therefore, although this model is a simplified model of a complex multiphysics system, in future work we plan to use this study framework to link the overall process step by step. In addition to our modeling approach enabling the reuse of constituents from existing models, the approach used here also allows future exploration of the effects seen here at the cellular level at the tissue and organ scale. For example, tools like OpenCMISS (Bradley et al., 2011) can directly integrate CellML models, like the one developed here, into electrophysiology and mechanical models and simulations at those larger scales (Nickerson et al., 2014).

Conclusion

In the present study, we exploit the model reuse capabilities of CellML, using individual components such as those described above. We constructed each constituent of the model separately. Once each simulation is validated, all numerical values using the CSV file were obtained. We plotted the behavior of the simulated components and justified them using experimental data. Then we

implemented the comprehensive electromechanical model by assembling these reusable modules *via* component instances and encapsulation hierarchies.

In addition, our model can reproduce the experimentally observed AP, Ca^{2+} transients, and force development as a function of temperature. The model could be useful in other related experiments and simulations.

The value of the current experimental study lies in the determination of both quantitative and qualitative differences between the left and right heart at different spatial levels. Findings that the fundamental properties of the myocardium differ between the left and right heart gives us an insight on which to base medical planning or interventions, using appropriate approaches for the two ventricles. This simple approach could allow one to account for phenomenological functions which are able to capture signal traces as well as the kinetic of tension development.

The current modeling study allowed the implementation and testing of each of the currents individually, providing a database of validated modular models (component models), which are available to reuse. To construct models by reusing components encoded with CellML enables computational efficiency and easy optimization. We successfully constructed the integrated cellular model by using a modular approach with CellML. This model, informed by the present experimental data, demonstrates well how the underlying mechanisms at a molecular level contribute to phenotype in higher levels, especially based on the description of the Ca^{2+} handling mechanism in the sarcoplasmic reticulum and the sarcolemmal membrane. This enables understanding of wall stress development in the left and right ventricles. Therefore, modeling is suggested as one of the best ways to assess both left and right ventricular function together, as the assessment of right ventricular function has previously been very difficult. This approach could allow one to account for the effect of certain drugs on cardiac functions.

Data availability statement

Publicly available datasets were analyzed in this study. This data can be found here: http://hdl.handle.net/2292/36950.

Ethics statement

All experimental procedures were performed according to the requirements of the Animal Ethics Committee of the University of Auckland (Approval R595 and R787) and the National Animal Ethics Advisory Committee (The Animal Welfare Act 1999, Schedules 1 to 7) as well as the protocol approved by the Institutional Review Board of Animals of Inje University College of Medicine.

Author contributions

NK and JP conceived and carried out the experiments. NK, AT, and PH designed the computer models. NK and DN developed and validated the computer models. NK wrote the manuscript. DN, AT, and PH read and reviewed the manuscript and approved the submitted version.

Conflict of interest

The authors declare that the research was conducted in the absence of any commercial or financial relationships that could be construed as a potential conflict of interest.

Publisher's note

All claims expressed in this article are solely those of the authors and do not necessarily represent those of their affiliated organizations, or those of the publisher, the editors and the reviewers. Any product that may be evaluated in this article, or claim that may be made by its manufacturer, is not guaranteed or endorsed by the publisher.

Supplementary material

The Supplementary Material for this article can be found online at: https://www.frontiersin.org/articles/10.3389/fphys.2022.965054/full#supplementary-material

References

Agus, Z. S., Dukes, I. D., and Morad, M. (1991). Divalent cations modulate the transient outward current in rat ventricular myocytes. *Am. J. Physiology-Cell Physiology* 261 (21), C310–C318. doi:10.1152/ajpcell.1991.261.2.C310

Allen, D. G., and Kentish, J. C. (1985). The cellular basis of the length-tension relation in cardiac muscle. *J. Mol. Cell. Cardiol.* 17 (9), 821–840. doi:10.1016/s0022-2828(85)80097-3

Alter, P., Rupp, H., Stoll, F., Adams, P., Figiel, J. H., Klose, K. J., et al. (2012). Increased enddiastolic wall stress precedes left ventricular hypertrophy in dilative heart failure-Use of the volume-based wall stress index. *Int. J. Cardiol.* 157 (2), 233–238. doi:10.1016/j.ijcard.2011.07.092

Apkon, M., and Nerbonne, J. M. (1991). Characterization of two distinct depolarization-activated K+ currents in isolated adult rat ventricular myocytes. *J. Gen. Physiol.* 97 (5), 973–1011. doi:10.1085/jgp.97.5.973

Berger, F., Borchard, U., Hafner, D., and Weis, T. M. (1998). Different inhibition patterns of tedisamil for fast and slowly inactivating transient outward current in rat ventricular myocytes. *Schmiedeb. Arch. Pharmacol.* 357 (3), 291–298. doi:10.1007/pl00005170

Bers, D. M. (2000). Calcium fluxes involved in control of cardiac myocyte contraction. *Circulation Res.* 87 (4), 275–281. doi:10.1161/01.res.87.4.275

Bers, D. M. (2002). Cardiac excitation-contraction coupling. *Nature* 415 (6868), 198–205. doi:10.1038/415198a

Bradley, C., Bowery, A., Britten, R., Budelmann, V., Camara, O., Christie, R., et al. (2011). OpenCMISS: A multi-physics & multi-scale computational infrastructure for the VPH/Physiome project. *Prog. Biophysics Mol. Biol.* 107 (1), 32–47. doi:10.1016/j.pbiomolbio.2011.06.015

Cerbai, E., Barbieri, M., and Mugelli, A. (1996). Occurrence and properties of the hyperpolarization-activated current I f in ventricular myocytes from normotensive and hypertensive rats during aging. *Circulation* 94 (7), 1674–1681. doi:10.1161/01.cir.94.7.1674

Chowienczyk, P., and Shah, A. (2012). Myocardial wall stress. *Hypertension* 60 (1), 10–11. doi:10.1161/HYPERTENSIONAHA.112.193839

Clark, R. B., Sanchez-Chapula, J., Salinas-Stefanon, E., Duff, H. J., and Giles, W. R. (1995). Quinidine-induced open channel block of K+ current in rat ventricle. *Br. J. Pharmacol.* 115 (2), 335–343. doi:10.1111/j.1476-5381.1995.tb15882.x

Clayton, R. H. (2001). Computational models of normal and abnormal action potential propagation in cardiac tissue: Linking experimental and clinical cardiology. *Physiol. Meas.* 22 (3), R15–R34. doi:10.1088/0967-3334/22/3/201

Cooling, M. T., Nickerson, D. P., Nielsen, P. M., and Hunter, P. J. (2016). Modular modelling with Physiome standards. *J. Physiol.* 594 (23), 6817–6831. doi:10.1113/JP272633

Crocini, C., and Gotthardt, M. (2021). Cardiac sarcomere mechanics in health and disease. *Biophys. Rev.* 13 (5), 637–652. doi:10.1007/s12551-021-00840-7

Danziger, R. S., Sakai, M., Lakatta, E. G., and Hansford, R. G. (1990). Interactive α- and β-adrenergic actions of norepinephrine in rat cardiac myocytes. *J. Mol. Cell. Cardiol.* 22 (1), 111–123. doi:10.1016/0022-2828(90)90976-9

Demir, S. S., Clark, J. W., Murphey, C. R., and Giles, W. R. (1994). A mathematical model of a rabbit sinoatrial node cell. *Am. J. Physiology-Cell Physiology* 266 (31), C832–C852. doi:10.1152/ajpcell.1994.266.3.C832

Farès, N., Bois, P., Lenfant, J., and Potreau, D. (1998). Characterization of a hyperpolarization-activated current in dedifferentiated adult rat ventricular cells in primary culture. *J. Physiol.* 506 (1), 73–82. doi:10.1111/j.1469-7793.1998.073bx.x

Garny, A., and Hunter, P. J. (2015). OpenCOR: A modular and interoperable approach to computational biology. *Front. Physiol.* 6, 26. doi:10.3389/fphys.2015.00026

Gillis, T. E., Marshall, C. R., Xue, X. H., Borgford, T. J., and Tibbits, G. F. (2000). Ca2+binding to cardiac troponin C: Effects of temperature and pH on mammalian and salmonid isoforms. *Am. J. Physiology-Regulatory, Integr. Comp. Physiology* 279 (5), R1707–R1715. doi:10.1152/ajpregu.2000.279.5.R1707

Granzier, H. L., and Irving, T. C. (1995). Passive tension in cardiac muscle: Contribution of collagen, titin, microtubules, and intermediate filaments. *Biophysical J.* 68 (3), 1027–1044. doi:10.1016/S0006-3495(95)80278-X

Grossman, W., Jones, D., and McLaurin, L. P. (1975). Wall stress and patterns of hypertrophy in the human left ventricle. *J. Clin. Invest.* 56 (1), 56–64. doi:10.1172/JCI108079

Han, J. C., Taberner, A. J., Kirton, R. S., Nielsen, P. M., Smith, N. P., and Loiselle, D. S. (2009). A unique micromechanocalorimeter for simultaneous measurement of heat rate and force production of cardiac trabeculae carneae. *J. Appl. Physiology* 107 (3), 946–951. doi:10.1152/japplphysiol.00549.2009

Hasenfuss, G., Reinecke, H., Studer, R., Meyer, M., Pieske, B., Holtz, J., et al. (1994). Relation between myocardial function and expression of sarcoplasmic reticulum Ca(2+)-ATPase in failing and nonfailing human myocardium. *Circ. Res.* 75 (3), 434–442. doi:10.1161/01.res.75.3.434

Hinch, R., Greenstein, J. L., Tanskanen, A. J., Xu, L., and Winslow, R. L. (2004). A simplified local control model of calcium-induced calcium release in cardiac ventricular myocytes. *Biophysical J.* 87 (6), 3723–3736. doi:10.1529/biophysj.104.049973

Hood, W. P., Jr., Rackley, C. E., and Rolett, E. L. (1968). Wall stress in the normal and hypertrophied human left ventricle. *Am. J. Cardiol.* 22 (4), 550–558. doi:10.1016/0002-9149(68)90161-6

Hudmon, A., Schulman, H., Kim, J., Maltez, J. M., Tsien, R. W., and Pitt, G. S. (2005). CaMKII tethers to L-type Ca2+ channels, establishing a local and dedicated integrator of Ca2+ signals for facilitation. *J. Cell Biol.* 171 (3), 537–547. doi:10.1083/jcb.200505155

Hunter, P. J., McCulloch, A. D., and ter Keurs, H. E. (1998). Modelling the mechanical properties of cardiac muscle. *Prog. Biophys. Mol. Biol.* 69 (2-3), 289–331. doi:10.1016/s0079-6107(98)00013-3

Jafri, M. S., Rice, J. J., and Winslow, R. L. (1998). Cardiac Ca2+ dynamics: The roles of ryanodine receptor adaptation and sarcoplasmic reticulum load. *Biophysical J.* 74 (3), 1149–1168. doi:10.1016/S0006-3495(98)77832-4

Janssen, P. M., Stull, L. B., and Marbán, E. (2002). Myofilament properties comprise the rate-limiting step for cardiac relaxation at body temperature in the rat. *Am. J. Physiology-Heart Circulatory Physiology* 282 (2), H499–H507. doi:10.1152/ajpheart.00595.2001

Kaprielian, R., Sah, R., Nguyen, T., Wickenden, A. D., and Backx, P. H. (2002). Myocardial infarction in rat eliminates regional heterogeneity of AP profiles,ItoK+currents, and [Ca2+]itransients. *Am. J. Physiology-Heart Circulatory Physiology* 283 (3), H1157–H1168. doi:10.1152/ajpheart.00518.2001

Kim, H. K., Kang, S. W., Jeong, S. H., Kim, N., Ko, J. H., Bang, H., et al. (2012). Identification of potential target genes of cardioprotection against ischemia-reperfusion injury by express sequence tags analysis in rat hearts. *J. Cardiol.* 60 (2), 98–110. doi:10.1016/j.jjcc.2012.02.004

Kim, N., Cannell, M. B., and Hunter, P. J. (2010). Changes in the calcium current among different transmural regions contributes to action potential heterogeneity in rat heart. *Prog. Biophysics Mol. Biol.* 103 (1), 28–34. doi:10.1016/j.pbiomolbio.2010.05.004

Kim, N. (2018). Multi-scale electromechanics of the heart. The University of Auckland. Doctoral Thesis.

Lee, H. C., Lu, T., Weintraub, N. L., VanRollins, M., Spector, A. A., and Shibata, E. F. (1999). Effects of epoxyeicosatrienoic acids on the cardiac sodium channels in isolated rat ventricular myocytes. *J. Physiology* 519, 153–168. doi:10.1111/j.1469-7793.1999.0153o.x

Li, Q., Cui, N., Du, Y., Ma, H., and Zhang, Y. (2013). Anandamide reduces intracellular Ca2+ concentration through suppression of Na+/Ca2+ exchanger current in rat cardiac myocytes. *PLoS One* 8 (5), e63386. doi:10.1371/journal.pone.0063386

Luo, C. H., and Rudy, Y. (1994). A dynamic model of the cardiac ventricular action potential. I. Simulations of ionic currents and concentration changes. *Circ. Res.* 74 (6), 1071–1096. doi:10.1161/01.res.74.6.1071

Lytton, J., Westlin, M., Burk, S. E., Shull, G. E., and MacLennan, D. H. (1992). Functional comparisons between isoforms of the sarcoplasmic or endoplasmic reticulum family of calcium pumps. *J. Biol. Chem.* 267 (20), 14483–14489. doi:10.1016/s0021-9258(19)49738-x

Mackiewicz, U., and Lewartowski, B. (2006). Temperature dependent contribution of Ca2+ transporters to relaxation in cardiac myocytes: Important role of sarcolemmal Ca2+-ATPase. *J. Physiol. Pharmacol.* 57 (1), 3–15.

McCubbin, W. D., Hincke, M. T., and Kay, C. M. (1980). The effect of temperature on some calcium-binding properties of troponin C and calmodulin. *Can. J. Biochem.* 58 (9), 683–691. doi:10.1139/o80-096

Milani-Nejad, N., and Janssen, P. M. (2014). Small and large animal models in cardiac contraction research: Advantages and disadvantages. *Pharmacol. Ther.* 141 (3), 235–249. doi:10.1016/j.pharmthera.2013.10.007

Miller, A. K., Marsh, J., Reeve, A., Garny, A., Britten, R., Halstead, M., et al. (2010). An overview of the CellML API and its implementation. *BMC Bioinforma.* 11, 178. doi:10.1186/1471-2105-11-178

Münch, G., Bölck, B., Karczewski, P., and Schwinger, R. H. (2002). Evidence for calcineurin-mediated regulation of SERCA 2a activity in human myocardium. *J. Mol. Cell. Cardiol.* 34 (3), 321–334. doi:10.1006/jmcc.2001.1515

Nickerson, D. P., Ladd, D., Hussan, J. R., Safaei, S., Suresh, V., Hunter, P. J., et al. (2014). Using CellML with OpenCMISS to simulate multi-scale Physiology. *Front. Bioeng. Biotechnol.* 2, 79. doi:10.3389/fbioe.2014.00079

Niederer, S. A., Hunter, P. J., and Smith, N. P. (2006). A quantitative analysis of cardiac myocyte relaxation: A simulation study. *Biophysical J.* 90 (5), 1697–1722. doi:10.1529/biophysj.105.069534

Pandit, S. V., Clark, R. B., Giles, W. R., and Demir, S. S. (2001). A mathematical model of action potential heterogeneity in adult rat left ventricular myocytes. *Biophysical J.* 81 (6), 3029–3051. doi:10.1016/S0006-3495(01)75943-7

Peiper, U., Laven, R., and Ehl, M. (1975). Force velocity relationships in vascular smooth muscle. *Pflugers Arch.* 356 (1), 33–45. doi:10.1007/BF00583519

Pitt, G. S., Zühlke, R. D., Hudmon, A., Schulman, H., Reuter, H., and Tsien, R. W. (2001). Molecular basis of calmodulin tethering and Ca2+-dependent inactivation of L-type Ca2+ channels. *J. Biol. Chem.* 276 (33), 30794–30802. doi:10.1074/jbc.M104959200

Puglisi, J. L., Bassani, R. A., Bassani, J. W., Amin, J. N., and Bers, D. M. (1996). Temperature and relative contributions of Ca transport systems in cardiac myocyte relaxation. *Am. J. Physiology-Heart Circulatory Physiology* 270 (52), H1772–H1778. doi:10.1152/ajpheart.1996.270.5.H1772

Stankovicova, T., Szilard, M., De Scheerder, I., and Sipido, K. R. (2000). M cells and transmural heterogeneity of action potential configuration in myocytes from the left ventricular wall of the pig heart. *Cardiovasc Res.* 45 (4), 952–960. doi:10.1016/s0008-6363(99)00418-6

Stein, R. B., Gordon, T., and Shriver, J. (1982). Temperature dependence of mammalian muscle contractions and ATPase activities. *Biophysical J.* 40 (2), 97–107. doi:10.1016/S0006-3495(82)84464-0

Stengl, M., Carmeliet, E., Mubagwa, K., and Flameng, W. (1998). Modulation of transient outward current by extracellular protons and Cd2+in rat and human ventricular myocytes. *J. Physiol.* 511 (3), 827–836. doi:10.1111/j.1469-7793.1998.827bg.x

Stimers, J. R., and Dobretsov, M. (1998). Adrenergic stimulation of Na/K pump current in adult rat cardiac myocytes in short-term culture. *J. Membr. Biol.* 163 (3), 205–216. doi:10.1007/s002329900384

Tandan, S., Wang, Y., Wang, T. T., Jiang, N., Hall, D. D., Hell, J. W., et al. (2009). Physical and functional interaction between calcineurin and the cardiac L-type Ca 2+ channel. *Circulation Res.* 105 (1), 51–60. doi:10.1161/CIRCRESAHA.109.199828

Taylor, D. G., Parilak, L. D., LeWinter, M. M., and Knot, H. J. (2004). Quantification of the rat left ventricle force and Ca2+-frequency relationships: Similarities to dog and human. *Cardiovasc. Res.* 61 (1), 77–86. doi:10.1016/j.cardiores.2003.09.022

Terkildsen, J. R., Niederer, S., Crampin, E. J., Hunter, P., and Smith, N. P. (2008). Using Physiome standards to couple cellular functions for rat cardiac excitation-contraction. *Exp. Physiol.* 93 (7), 919–929. doi:10.1113/expphysiol.2007.041871

Toyofuku, T., Curotto Kurzydlowski, K., Narayanan, N., and MacLennan, D. H. (1994). Identification of Ser38 as the site in cardiac sarcoplasmic reticulum Ca(2+)-ATPase that is phosphorylated by Ca2+/calmodulin-dependent protein kinase. *J. Biol. Chem.* 269 (42), 26492–26496. doi:10.1016/s0021-9258(18)47221-3

Volk, T., Nguyen, T. H., Schultz, J. H., and Ehmke, H. (1999). Relationship between transient outward K + current and Ca 2+ influx in rat cardiac myocytes of endo- and epicardial origin. *J. Physiology* 519, 841–850. doi:10.1111/j.1469-7793.1999.0841n.x

Walker, L. A., and Buttrick, P. M. (2009). The right ventricle: Biologic insights and response to disease. *Ccr* 5 (1), 22–28. doi:10.2174/157340309787048077

Weis, T., Berger, F., and Borchard, U. (1993). A slowly inactivating transient outward current in rat ventricular myocytes. *Pflugers Arch.* 425 (1-2), 184–186. doi:10.1007/BF00374522

Wettwer, E., Amos, G., Gath, J., Zerkowski, H. R., Reidemeister, J. C., and Ravens, U. (1993). Transient outward current in human and rat ventricular myocytes. *Cardiovasc. Res.* 27 (9), 1662–1669. doi:10.1093/cvr/27.9.1662

Wier, W. G., Egan, T. M., López-López, J. R., and Balke, C. W. (1994). Local control of excitation-contraction coupling in rat heart cells. *J. Physiol.* 474 (3), 463–471. doi:10.1113/jphysiol.1994.sp020037

Yin, F. C. (1981). Ventricular wall stress. *Circ. Res.* 49 (4), 829–842. doi:10.1161/01.res.49.4.829

Zahradníková, A., Kubalová, Z., Pavelková, J., Györke, S., and Zahradník, I. (2004). Activation of calcium release assessed by calcium release-induced inactivation of calcium current in rat cardiac myocytes. *Am. J. Physiology-Cell Physiology* 286 (2), C330–C341. doi:10.1152/ajpcell.00272.2003